Radiocarbon dating of lime plaster from a Roman period cistern in ancient Gerasa, Jerash in Jordan

Daugbjerg, Thomas Schrøder; Lichtenberger, Achim; Lindroos, Alf; Michalska, Danuta; Raja, Rubina; Olsen, Jesper

Published in:
Journal of archaeological science: Reports

DOI:
10.1016/j.jasrep.2022.103373

Published: 01/04/2022

Document Version
Final published version

Journal of Archaeological Science: Reports 42 (2022) 103373

Contents lists available at ScienceDirect

Journal of Archaeological Science: Reports

journal homepage: www.elsevier.com/locate/jasrep

Radiocarbon dating of lime plaster from a Roman period cistern in ancient Gerasa, Jerash in Jordan

Thomas Schrøder Daugbjerg [a,b,*], Achim Lichtenberger [c], Alf Lindroos [d], Danuta Michalska [e], Rubina Raja [b,f], Jesper Olsen [a,b]

[a] Aarhus AMS Centre (AARAMS), Department of Physics and Astronomy, Aarhus University, Aarhus, Denmark
[b] Centre for Urban Network Evolutions (UrbNet), Moesgård Allé 20, DK-8270 Højbjerg, Aarhus University, Denmark
[c] Institut für Klassische Archäologie und Christliche Archäologie/Archäologisches Museum, University of Münster, Germany
[d] Faculty of Science and Technology, Åbo Akademi University, Turku, Finland
[e] Institute of Geology, Faculty of Geographic and Geological Sciences, Adam Mickiewicz University, Poznan, Poland
[f] Department of History and Classical Studies, School of Culture and Society, Aarhus University, Denmark

ARTICLE INFO

Keywords:
Gerasa
Jerash
Jordan
Roman period
Water management
Mortar dating
Stepwise injection

ABSTRACT

Ancient Gerasa (Jerash, since the Islamic period) is a city with a rich archaeological heritage from prehistory onwards, with the periods from Roman times into the Early Islamic period best attested. A Danish-German team has been working in the Northwest Quarter of the city since 2011. Among the findings was a Roman period monumental cistern that was intentionally filled in, at one point in time. The complexity of the archaeology raised chronological questions regarding the construction, destruction and subsequent backfilling of the cistern. This study contributed to answer these questions by radiocarbon dating lime plaster excavated from the cistern, and comparing the results with charcoal radiocarbon dates from other studies. Radiocarbon dating of plaster and mortar in Jerash is challenging because of contamination of geological carbonates from the local limestone geology. Quoting previous mortar dating studies, this study utilized sample characterization by alkalinity screening, petrography, SEM-EDS, and sample pre-treatment and preparation by wet sieving, sedimentation and stepwise injection. The plaster dates argued for the construction of the cistern being in the last half of the 1st century BCE to the middle of the 1st century CE. A few samples had later mortar dates, which argued for the filling event of the cistern taking place sometime in the late 3rd century CE or later.

1. Introduction

The ancient city of Gerasa was part of the Roman Decapolis, a group of nominally ten cities (Lichtenberger, 2003; Raja, 2012). From the Islamic period onwards, Gerasa has been known by its Arabic name Jerash. Archaeological findings outside the modern city show that the site was occupied by humans even far back in prehistorical times (al-Nahar, 2010; al-Nahar, 2018), and it has been characterized as a so-called mega-site. Most archaeological remains, however, stem from the Roman (63 BCE–400 CE), Byzantine (400–640 CE) and Early Islamic (640–749 CE) periods, when the city flourished with extensive residential areas, public buildings and monuments (Kennedy, 2007; Raja, 2012; Seigne, 1992; Thomsen, 2019). A devastating earthquake in January 749 CE put a halt to the development of the city, and at least in the Northwest Quarter habitation is only found again in the Middle Islamic period (10th–15th centuries CE) (Lichtenberger and Raja, 2016a; Lichtenberger and Raja, 2018). From the 1920s to the present, international excavations have explored the archaeological record of Jerash (Kraeling, 1938; Zayadine, 1986). Throughout the 20th century, a modern city sprawled east of the river of the city covering almost half of the ancient city, only leaving the western part, which is a protected archaeological site, visible (Lichtenberger et al., 2019; Stott et al., 2018).

The abundant archaeological record of Jerash offers great potential for studying urban life in the Roman, Byzantine and Early Islamic periods. The Danish-German Jerash Northwest Quarter Project has investigated the Northwest Quarter of Jerash (Fig. 1), a peripheral area of the ancient city, but which features residential houses and building complexes for production purposes as well as cisterns and a church, which earlier had been a synagogue. The Northwest Quarter is the highest area

* Corresponding author at: Aarhus AMS Centre, Department of Physics and Astronomy, Aarhus University, Ny Munkegade 120, DK-8000 Aarhus C, Denmark.
E-mail address: thomas.daugbjerg@phys.au.dk (T.S. Daugbjerg).

https://doi.org/10.1016/j.jasrep.2022.103373
Received 27 May 2021; Received in revised form 4 February 2022; Accepted 5 February 2022
Available online 4 March 2022

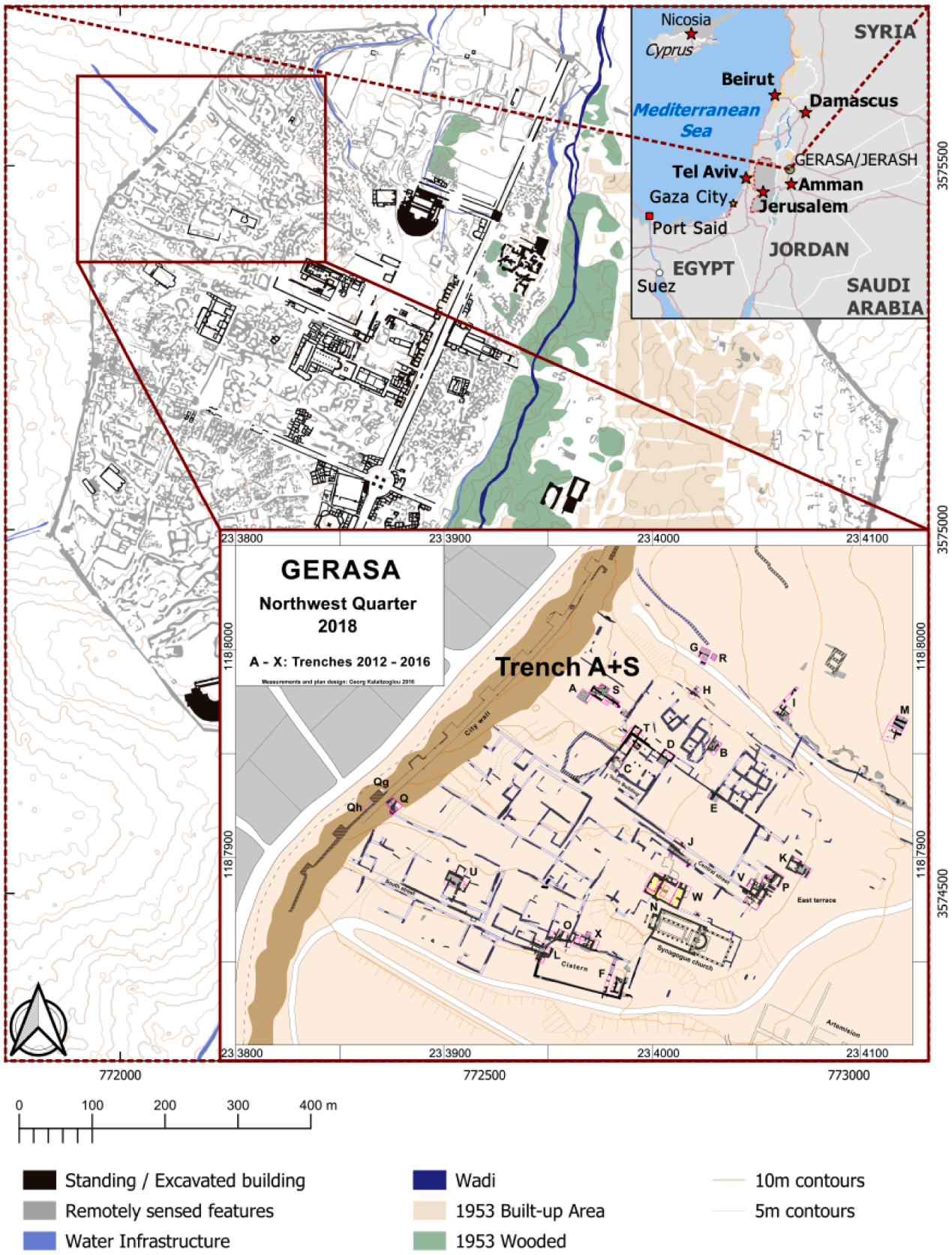

Fig. 1. Map of the Northwest Quarter, Gerasa/Jerash and the Middle East. The Roman era building with cistern is located in Trench A and Trench S. (Maps credit: Danish-German Jerash Northwest Quarter Project).

Fig. 2. Photograph from Trench S. (Photo credit: Danish-German Jerash Northwest Quarter Project). View of the staircase leading into the cistern. To the right in the photo the settling basin is visible. Pilasters are visible on both sides of the cistern chamber.

within the walled city of ancient Gerasa, and its position in the northwestern part of the city explains the prominent role this area had for water supply of the Roman city. Important water sources were situated to the northwest of the city, water was brought into the city, and the Northwest Quarter as the most elevated area of the city served for distribution of the water into lower parts of the city. Therefore, it does not come as a surprise that two large water reservoirs were found in this area (Lichtenberger and Raja, 2020b; Boyer, 2019; Lichtenberger and Raja, 2016b; Seigne, 2004).

Trench A and Trench S hold part of a Roman period cistern, which had a contemporary building located on top (Figs. 1 and 2). The complex was situated on the highest point within the Northwest Quarter and must have belonged to a prominent construction dating to the Roman period. The building was at some point in the Late Roman period (250–400 CE) intentionally destroyed and dismantled to its foundations, and the cistern was back-filled. The building and cistern were part of an elaborate Roman period complex, but the layout and therefore function of the complex as well as the reason for its destruction are not clear (Lichtenberger and Raja, 2015). The excavation in Trench S uncovered part of the well-constructed cistern, pilasters in the cistern, remains of arches spanning the cistern, a semi-circular settling basin, an entrance staircase that led into the cistern and decorative wall paintings. In the fill of the cistern, further fragments of painted walls and stucco elements were found, along with other finds thrown into the fill at the time when the cistern was closed off. This study aimed to date the original establishment of the structure with a higher degree of certainty, as well as the intentional closure of the complex. Both events have an impact on the way in which we can view the cultural history of the site and situate it better and firmer within its regional and Roman imperial contexts.

However, it is a challenge for absolute dating in Jerash that undisturbed archaeological strata are rare due to the long and often uninterrupted human activities at the site. This is because of the site's intensive human activity for nearly a millennium, and the frequent earthquakes in the region, which would have destroyed parts of the city that then would have needed rebuilding, involving filling-in and levelling. Furthermore, the typology and relative chronology of the local pottery, which was predominant throughout more than 500 years, did not change immensely across the centuries and therefore cannot be used as firm indicators of dating of archaeological strata (Kehrberg, 2001; Lichtenberger and Raja, 2020a; Uscatescu, 1996). Therefore, refined methods for constructing optimised chronologies were urgently needed for an improved understanding of urban development at Jerash. Consequently, this study attempted radiocarbon dating of plaster samples from the building with cistern excavated in Trench S.

Radiocarbon dating of lime plaster and lime mortar works by exploiting that the hardening-process of lime absorbs atmospheric CO_2 (Heinemeier et al., 2010; Labeyrie and Delibrias, 1964; Ringbom et al., 2014; Stuiver and Smith, 1965). Lime production starts by firing limestone above 900 °C where the constituent calcite ($CaCO_3$) decomposes to quicklime (CaO). The production then mixes quicklime and water to make slaked lime ($Ca(OH)_2$). Finally, one mixes slaked lime and an aggregate material, typically sand, and the wet lime-based material is ready for use as plaster or mortar in construction. Lime plaster and lime mortar harden through a chemical reaction were slaked lime absorbs atmospheric CO_2 and transforms back to calcite ($CaCO_3$), which is the lime binder of the material. In this way, the lime binder captures the atmospheric ^{14}C signal at the time of hardening, and it is feasible to radiocarbon date lime plaster and lime mortar for the time of hardening. In this study, mortar dating refers to radiocarbon dating of both plaster and mortar.

Mortar dating sometimes yields inconclusive results, when samples have contaminants that are similar to the lime binder dating material ($CaCO_3$) (Heinemeier et al., 2010; Lindroos et al., 2018; Ringbom et al., 2014). See the materials and methods section for further explanation of criteria for conclusive and inconclusive mortar dating results. One example of contaminants that can cause inconclusive results is secondary carbonates, if the binder calcite acts as an open system that exchanges carbon with the surroundings throughout the lifetime of the mortar (Boaretto, 2009; Daugbjerg et al., 2021; MacLeod et al., 1991; Nawrocka et al., 2009). Another example is geological carbonate, containing no ^{14}C atoms, which can come from grains of limestone ($CaCO_3$) in the aggregate or an incomplete lime burning (Baxter and Walton, 1970; Labeyrie and Delibrias, 1964; Stuiver and Smith, 1965).

Lichtenberger et al. (2015) already radiocarbon dated mortar from a Roman period cistern on the south slope of the Northwest Quarter of Jerash (see Trench F in Fig. 1). That work obtained many inconclusive results as some samples had secondary carbonates and all samples had geological carbonate from aggregate limestone grains. Most likely, mortar production used local sediments as aggregate for the mortar of Jerash. The geology and sediments at Jerash are rich in limestone formations and limestone grains (Abed, 1982; Bender, 1974), and a petrographic study found limestone sand and gravel in Jerash mortar aggregate (Yaseen et al., 2013). These contaminants make mortar dating in Jerash challenging.

However, Daugbjerg et al. (2022) employed a specialised mortar dating preparation technique based on sedimentation and stepwise injection, and compared to sequential dissolution in Lichtenberger et al. (2015) this improved discrimination against contaminating geological carbonate for Jerash mortar. Here we report on applying this method of mortar dating with a focus on decorative wall plaster and stucco excavated in Trench S.

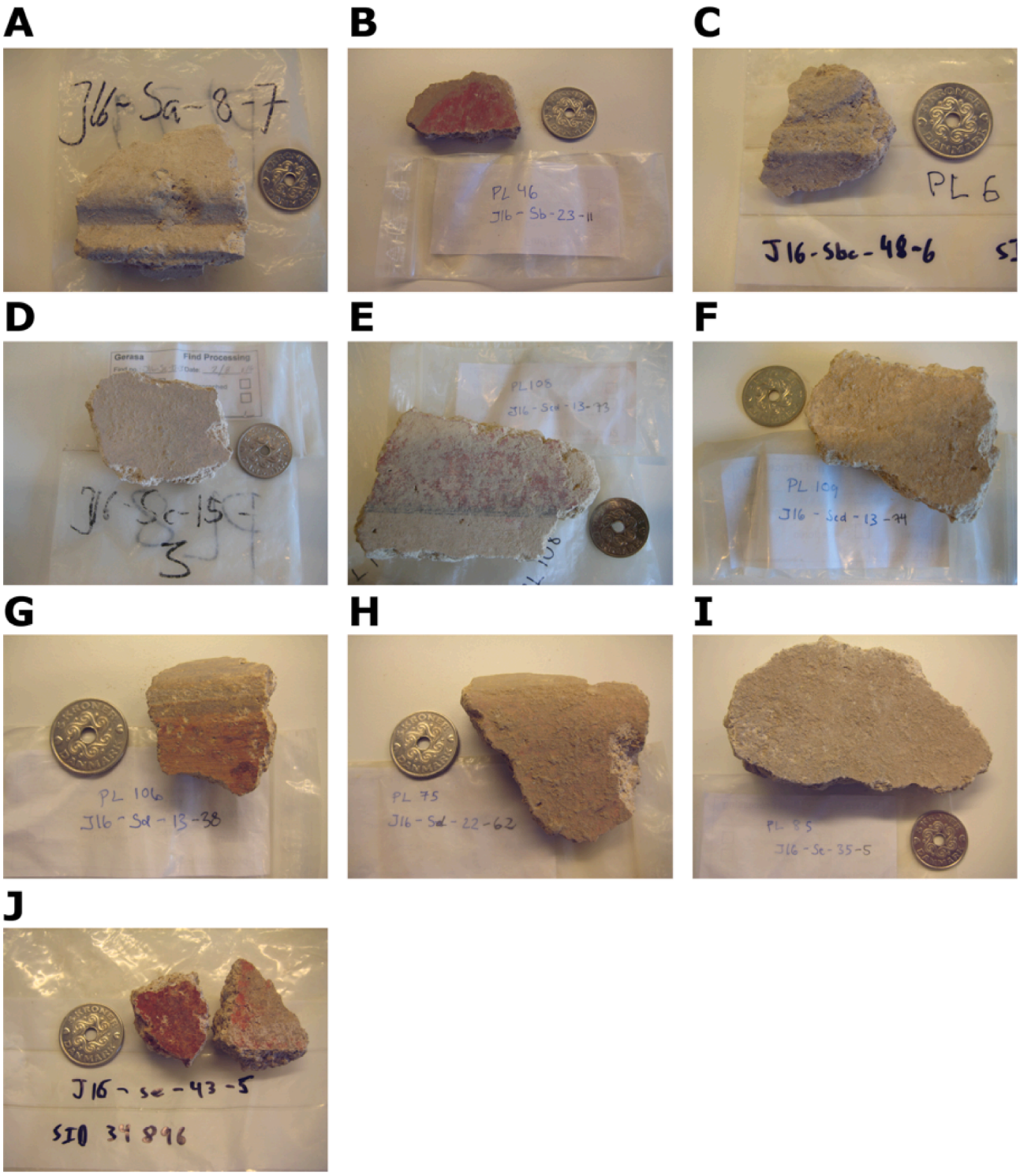

Fig. 3. Photographs of plaster samples from the Roman era building with cistern in Trench S. The coin "5 kroner" had a diameter of 28.5 mm. Thomsen (2019) has further sample descriptions. **A** J16-Sa-8-7, plaster. **B** J16-Sb-23-11, painted plaster. **C** J16-Sbc-48-6, plaster with curved texture. **D** J16-Sc-15-3, plaster. **E** J16-Scd-13-73, painted plaster. **F** J16-Scd-13-74, plaster. **G** J16-Sd-13-38, painted plaster. **H** J16-Sd-22-62, painted plaster. **I** J16-Se-35-5, plaster. **J** Sample J16-Se-43-5, painted plaster.

Table 1
List of 10 plaster samples from the Roman building with cistern excavated in Trench S. The table lists various information from pre-treatment, preparation method, characterization, radiocarbon dating of CO_2 fractions and conclusive mortar dates. Materials and methods explained the conclusiveness criteria, and profiles with 'Failed the criteria' in the 'Conclusiveness criteria' column did not pass any of the criteria. The derived conclusive mortar dates are in the column 'Conclusive age'. The three stable calcite references of alkalinity characterization determined the alkalinity standard with their weighted average $\Delta pH/m = (17.3 \pm 0.8)\ 10^{-3}$ pH/mg.

Sample Material Preparation method	**Geo. C in petrography** Alkalinity, ΔpH/m (10^{-3} pH/mg) χ^2 test alkalinity	**Grain fraction** Carbon yield (%) Mass (mg)	Laboratory no.	Reaction time (s)	Cumulative CO_2 fraction	^{14}C age (^{14}C years BP)	δ13C AMS ‰ VPDB	Conclusiveness criteria	**Conclusive age** χ2-test (^{14}C years BP)
J16-Sa-8–7	**Abundant**	**<10 μm**	AAR-33417.SI1.1	240	0–0.0180	1488 ± 29	−20	Failed the criteria	**–**
Plaster	17 ± 2	12 %	AAR-33417.SI1.2	660	0.0180–0.0378	1684 ± 26	−13		–
Stepwise injection	df = 1 T = 0.0(5% 3.8)	165.2 mg	AAR-33417.SI1.3	1080	0.0378–0.0603	1734 ± 28	−14		
			AAR-33417.SI1.4	1530	0.0603–0.0829	1757 ± 32	−14		
J16-Sb-23–11	**Abundant**	**<10 μm**	AAR-33418.SI1.1	300	0–0.0200	2088 ± 33	−18	CIII	**2051 ± 38**
Plaster	18 ± 1	10 %	AAR-33418.SI1.2	900	0.0200–0.0392	2279 ± 32	−14	(J16-Scd-13–73)	(mean ± std)
Stepwise injection	df = 1 T = 0.4(5% 3.8)	199.7 mg	AAR-33418.SI1.3	1320	0.0392–0.0584	2665 ± 34	−13		df = 1 T = 2.2(5% 3.8)
			AAR-33418.SI1.4	1800	0.0584–0.0803	2629 ± 44	−14		
J16-Sbc-48–6	**Abundant**	**<10 μm**	AAR-33419.SI1.1	300	0–0.0363	1671 ± 32	−19	Failed the criteria	**–**
Plaster	17 ± 2	11 %	AAR-33419.SI1.2	720	0.0363–0.0668	1859 ± 30	−15		–
Stepwise injection	df = 1 T = 0.0(5% 3.8)	102.6 mg	AAR-33419.SI1.3	1320	0.0668–0.0843	1949 ± 36	−15		
			AAR-33419.SI1.4	1740	0.0843–0.103	1956 ± 43	−17		
J16-Sc-15–3	**Abundant**	**<10 μm**	AAR-33420.SI1.1	270	0–0.0183	1718 ± 30	−17	CI	**1735 ± 24**
Plaster	19 ± 2	13 %	AAR-33420.SI1.2	810	0.0183–0.0368	1761 ± 38	−15	CI	(weighted average)
Stepwise injection	df = 1 T = 0.4(5% 3.8)	155.3 mg	AAR-33420.SI1.3	1380	0.0368–0.0551	1919 ± 34	−15		df = 1 T = 0.8(5% 3.8)
			AAR-33420.SI1.4	1950	0.0551–0.0752	2038 ± 35	−16		
J16-Scd-13–73	**Highly abundant**	**<10 μm**	AAR-33421.SI1.1	240	0–0.0189	2013 ± 39	−22	CIII	**1983 ± 30**
Plaster	17 ± 2	13 %	AAR-33421.SI1.2	630	0.0189–0.0380	2187 ± 39	−18	(J16-Se-43–5)	(mean ± std)
Stepwise injection	df = 1 T = 0.0(5% 3.8)	96.0 mg	AAR-33421.SI1.3	1110	0.0380–0.0640	2183 ± 44	−20		df = 1 T = 1.5(5% 3.8)
			AAR-33421.SI1.4	1560	0.0640–0.0885	2374 ± 33	−20		
J16-Scd-13–74	**Abundant**	**<10 μm**	AAR-33422.SI1.1	240	0–0.0186	2508 ± 33	−17	Decreasing	**–**
Plaster	19 ± 2	13 %	AAR-33422.SI1.2	780	0.0186–0.0435	2485 ± 31	−14	profile:	–
Stepwise injection	df = 1 T = 0.5(5% 3.8)	155.4 mg	AAR-33422.SI1.3	1260	0.0435–0.0701	2385 ± 27	−14	Disqualified!	
			AAR-33422.SI1.4	1740	0.0701–0.0967	2427 ± 31	−15		
J16-Sd-13–38	**Highly abundant**	**<10 μm**	AAR-33423.SI1.1	300	0–0.0212	2198 ± 29	−20	Failed the criteria	**–**
Plaster	18 ± 1	12 %	AAR-33423.SI1.2	840	0.0212–0.0442	2347 ± 28	−12		–
Stepwise injection	df = 1 T = 0.4(5% 3.8)	164.9 mg	AAR-33423.SI1.3	1410	0.0442–0.0726	2497 ± 29	−13		
			AAR-33423.SI1.4	2010	0.0726–0.0963	2550 ± 28	−15		
J16-Sd-22–62	**Abundant**	**<10 μm**	AAR-33424.SI1.1	240	0–0.0174	2103 ± 32	−19	CIII	**2058 ± 45**
Plaster	17 ± 2	13 %	AAR-33424.SI1.2	750	0.0174–0.0383	2310 ± 32	−15	(J16-Scd-13–73)	(mean ± std)
Stepwise injection	df = 1 T = 0.0(5% 3.8)	155.2 mg	AAR-33424.SI1.3	1230	0.0383–0.0638	2474 ± 34	−17		df = 1 T = 3.2(5% 3.8)
			AAR-33424.SI1.4	1680	0.0638–0.0902	2534 ± 29	−16		

(*continued on next page*)

Table 1 (*continued*)

Sample	**Geo. C in petrography**	**Grain fraction**	Laboratory no.	Reaction time (s)	Cumulative CO_2 fraction	^{14}C age (^{14}C years BP)	δ13C AMS ‰ VPDB	Conclusiveness criteria	**Conclusive age**
Material	Alkalinity, ΔpH/m (10^{-3} pH/mg)	Carbon yield (%)							χ2-test (^{14}C years BP)
Preparation method	χ^2 test alkalinity	Mass (mg)							
J16-Se-35–5	**Highly abundant**	**<10 μm**	AAR-33425.SI1.1	300	0–0.0219	1639 ± 28	−20	CI	**1663 ± 24**
Plaster	16 ± 1	13 %	AAR-33425.SI1.2	840	0.0219–0.0420	1687 ± 32	−19	CI	(mean ± std)
Stepwise injection	df = 1 T = 1.1(5% 3.8)	155.6 mg	AAR-33425.SI1.3	1380	0.0420–0.0712	1909 ± 27	−18		df = 1 T = 1.3(5% 3.8)
			AAR-33425.SI1.4	1920	0.0712–0.0984	1881 ± 29	−19		
J16-Se-43–5	**Highly abundant**	**<10 μm**	AAR-33426.SI1.1	300	0–0.0201	1953 ± 31	−19	CI	**1967 ± 22**
Plaster	18 ± 1	12 %	AAR-33426.SI1.2	840	0.0201–0.0399	1980 ± 31	−17	CI	(weighted average)
Stepwise injection	df = 1 T = 0.7(5% 3.8)	165.4 mg	AAR-33426.SI1.3	1380	0.0399–0.0591	2068 ± 28	−17		df = 1 T = 0.4(5% 3.8)
			AAR-33426.SI1.4	1920	0.0591–0.0830	2047 ± 30	−16		

2. Materials and methods

2.1. Samples

Fig. 3 shows the ten plaster samples from the Roman period building with cistern where the age is unknown (see Table 1 for a list of samples). The selected samples have a distinct smooth surface, they are pieces of stucco or plaster, and many of them are decoratively painted. Likely origins for these samples are wall surfacing that hardened with good atmospheric contact, so the risk of delayed hardening is low (Daugbjerg et al., 2021).

2.2. Sample pre-treatment

A hammer and chisel separated surface pieces with limited thicknesses, i.e. thickness from 1.1 cm to 2.6 cm, and mass from 23.4 g to 59.7 g. A coarse brush followed by a soft brush cleaned samples of sand and sediment. Cryogenic breaking froze and thawed samples five times, and each cycle exposed the sample to 1 minute in liquid nitrogen and 5 minutes in an 80 °C oven (Marzaioli et al., 2013; Nawrocka et al., 2005). The freezing and thawing aimed to stress the lime binder of the mortar and increase the amount of binder grains produced when the sample was crushed.

Pliers crushed the sample with just enough force to crumble it and no more, as excessive force could have crushed contaminating aggregate material (Heinemeier et al., 2010). By hand shaking for 20 minutes, a tower of test sieves dry sieved the crushed sample to obtain several grain size fractions from 100 μm to 500 μm (Van Strydonck et al., 1986; Van Strydonck et al., 1992). Using ultrapure water (Millipore E.M.D., 2013) in a spray bottle, the grain size fractions smaller than 125 μm were wet sieved, and this produced several grain size fractions from <38 μm to 125 μm. Finally, sedimentation of the <38 μm grain size fraction in a column of ultrapure water produced a grain size fraction <10 μm for radiocarbon dating (Daugbjerg et al., 2022). All available <38 μm grain size fraction (typically 0.4–3.0 g) was dispersed in the water column, and typically 0.1–0.5 g of <10 μm material was recovered from the water column. In this procedure, the ratio of <10 μm material to <38 μm material was sample dependent with typical values from 7 % to 12 %. If the <38 μm grain size fraction was in the lower range of the typical amount, the sedimentation was repeated one or three additional times to obtain enough <10 μm material for radiocarbon dating.

2.3. Sample characterization

Sample characterization assessed the sample alkalinity, which is one indicator for secondary carbonates (Heinemeier et al., 1997; Lichtenberger et al., 2015; Lindroos et al., 2007). First, a pH electrode (WTW, 2017) was placed in 10 mL ultrapure water without the sample, and it measured pH as the mean and standard deviation of measurements every fifth minute from 15 minutes to 60 minutes of submersion. Then, about 200 mg of the 125–250 μm grain size fraction from dry-sieving was added to the ultrapure water, and there was a similar pH measurement. This enabled calculating a pH shift per mass of sample, denoted ΔpH/m, which quantified alkalinity. Three batches of approximately 200 mg crushed calcite crystal had similar ΔpH/m measurements, and these had a weighted average with uncertainty calculated to provide a standard for stable calcite. To establish a threshold for unacceptable sample alkalinity, a weighted average was calculated for the ΔpH/m of a sample and the stable calcite standard. If this weighted average failed a chi-square test for goodness of fit (Bennett and Franklin, 1954; Press et al., 1992) the sample was ruled significantly alkaline and unsuited for mortar dating (the critical value is $\chi^2(df = 1, \alpha = 5\%) = 3.8$).

Notice that the alkalinity test used the grain size fraction 125–250 μm, which was different from the <10 μm grain size fraction used for stepwise injection and radiocarbon dating as presented later in this section. This study used the idea of characterizing alkalinity with one of

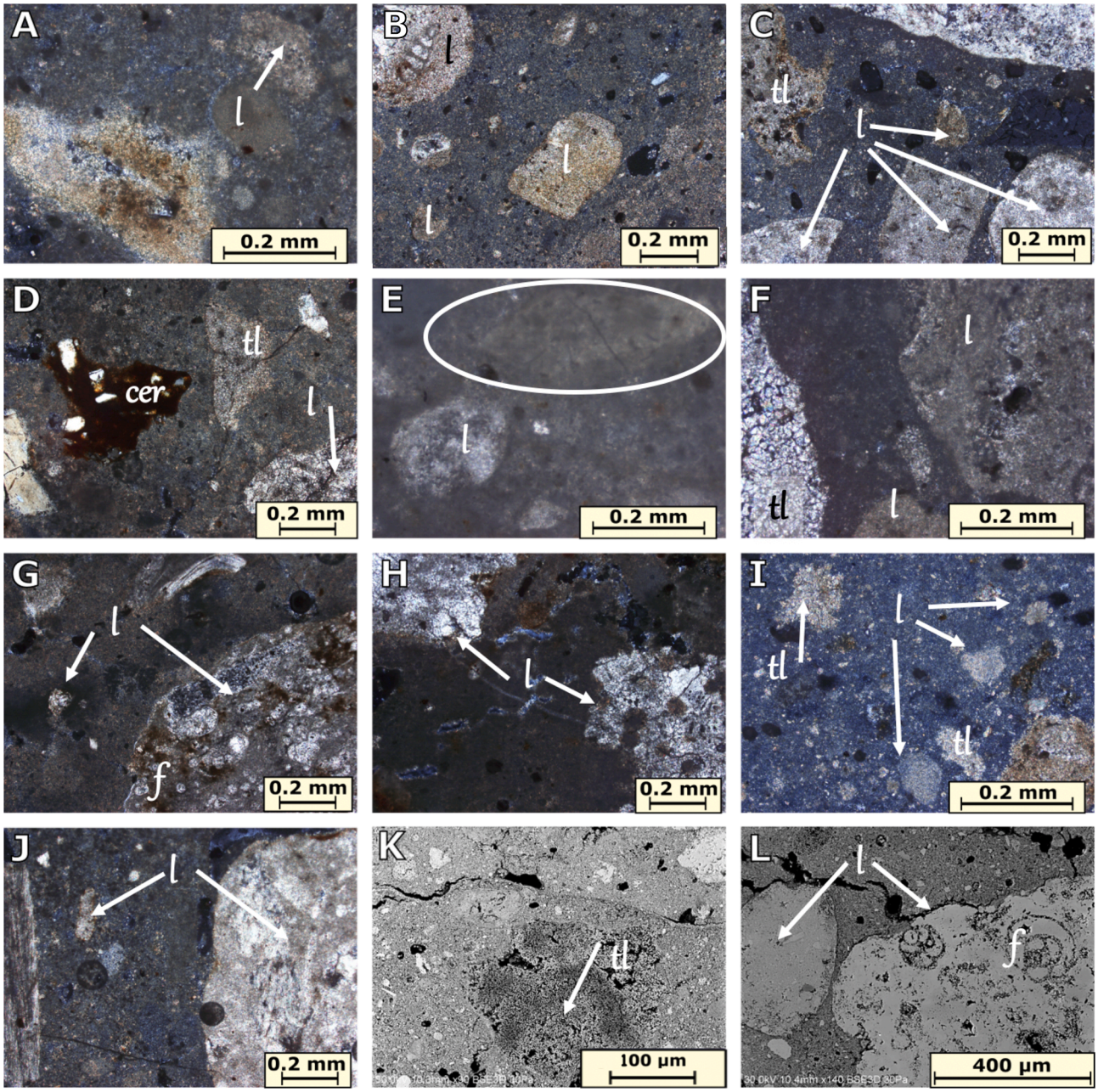

Fig. 4. Microphotograph of carbonaceous components of samples (geological carbonate source in the context of the ^{14}C measurements results). **A-J** Polarizing light microscopic view, XN. **K-L** SEM photo of selected samples. Petrographic identifications: f- foraminifera; l- carbonaceous components; tl- thermally changed carbonaceous components; cer- ceramic fragments. **A** Non-homogeneous binder of sample J16-Sa-8-7, with limestone aggregate fragments partially burnt and sparitic calcite stained with iron oxides (lower-left corner). This stained sparitic calcite is likely to be secondary. **B** Sample J16-Sb-23-11, not totally burnt carbonaceous fragments of aggregate and bioclastic limestone on the upper left corner. **C** Sample J16-Sbc-48-6, a large amount of carbonate aggregate, very small (<0.25 µm) pieces of limestone visible in the binder. **D** Sample J16-Sc-15-3, thermally changed, small carbonaceous fragments and pieces of crushed ceramics. **E** Sample J16-Scd-13-73, not totally burnt carbonaceous fragments (marked with the circle). **F** Sample J16-Scd-13-74, a large amount of carbonate aggregate (marl, dolomite), partially thermally changed. **G** Sample J16-Sd-13-38, large bioclastic limestone fragment, shell and small carbonaceous fragments within the binder. **H** Sample J16-Sd-22-62, carbonaceous fragments of aggregate and lime binder with higher amount of clay minerals within the binder. **I** Sample J16-Se-35-5, rich in geological carbonate, a lot of carbonate aggregate, including numerous incomplete burned fragments. **J** Sample J16-Se-43-5, a large fragment of carbonate aggregate, shells and numerous small fragments of not fully burnt limestone. **K** Sample J16-Scd-13-74, porous disintegrated lime grain in the centre. **L** Sample J16-Sd-22-62, bioclastic limestone.

the smaller dry sieved grain fractions, which some studies have used as a proxy for the alkalinity of a sample and its derived grain fractions (Lichtenberger et al., 2015; Lindroos et al., 2011; Lindroos et al., 2020; Tirelli et al., 2020). One could consider the advantages of alkalinity characterizing the same grain fraction as used for radiocarbon dating. However, there may be a problem in alkalinity characterizing grain fractions from wet sieving or sedimentation, as the water used in these pre-treatment methods may carry off some of the alkalinity prior to the alkalinity characterization (Daugbjerg et al., 2021; Lindroos et al., 2007; MacLeod et al., 1991). Therefore, we did not try the latter approach.

Petrography and SEM-EDS characterized the mineralogy of the samples and the presence of geological carbonate and secondary carbonate (Goslar et al., 2009; Michalska, 2019; Tirelli et al., 2020; Toffolo et al., 2020). The mineralogical examination of the components (binder and aggregate) of the sample was carried out through a polarizing light microscope Olympus AX 70-Prons. The investigation of the

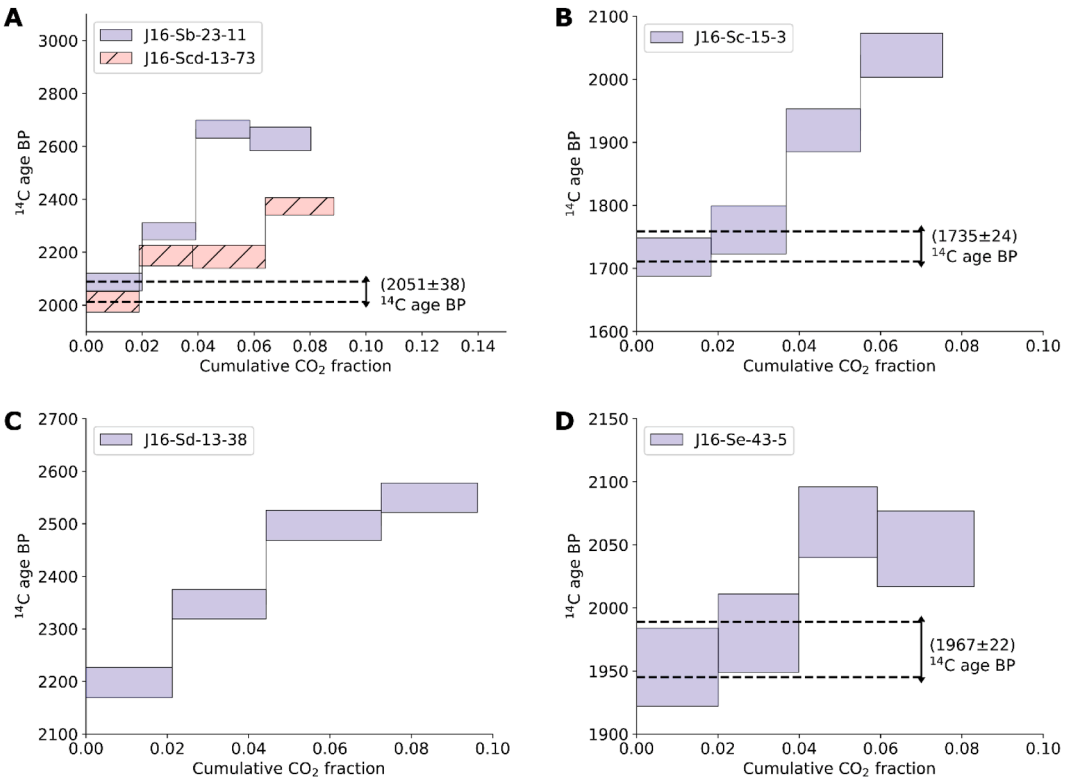

Fig. 5. Examples of radiocarbon profiles from the Roman period building in Trench S. Materials and methods explained the conclusiveness criteria. **A** Samples J16-Sb-23-11 and J16-Scd-13-73, and their criterion III age: (2051 ± 38) ^{14}C age BP. **B** Sample J16-Sc-15-3 and criterion I age: (1735 ± 24) ^{14}C age BP. **C** Sample J16-Sd-13-38 had an inconclusive radiocarbon profile **D** Sample J16-Se-43-5 and criterion I age: (1967 ± 22) ^{14}C age BP.

microstructure and chemical composition of binder and aggregate were studied by scanning electron microscope Hitachi S-3700N coupled with energy dispersive X-ray spectrometer (SEM-EDS). Thin sections and SEM-EDS analyses were made at the Institute of Geology, Adam Mickiewicz University, Poznań, Poland.

2.4. Stepwise injection and radiocarbon analysis

Stepwise injection refers to a method where addition of diluted acid for generating CO_2 for radiocarbon analysis is added stepwise (see Al-Bashaireh (2013, 2015), Daugbjerg et al. (2022) and Van Strydonck et al. (1986, 1992)). Prior to stepwise injection, 85 % H_3PO_4 totally dissolved a small sample aliquot (approximately 10 mg) to determine the carbon yield, see Table 1. Using the predetermined carbon yield, another sample aliquot was made with mass scaled so five 0.4 mgC fractions covered the first 10 % of the total carbon content of the aliquot. In this scaling, the goal was to cover the first 10 % of the total carbon content with 5 fractions and thereby focus on the most rapidly dissolving material that is crucial for dating (Folk and Valastro, 1976). The value of fraction size 0.4 mgC was a compromise between reducing the amount of pre-treated material needed for stepwise injection, while also avoiding AMS radiocarbon dating very small samples (0.1 mgC) that are associated with higher uncertainty for the ^{14}C age determination (Olsen et al., 2017; Stuiver and Polach, 1977). Following the scaling of mass of pre-treated material, stepwise injection suspended this material in ultrapure water in a reactor flask. A vacuum system evacuated the reactor flask, but the contained water kept a certain pressure of water vapor in the reactor. A burette then injected batches of approximately 2.0 mL of $3.0{\cdot}10^{-2}$ mol/L H_3PO_4. When injected, the acid reacted with the suspended sample powder and released CO_2. When the reaction had consumed the acid, it stopped.

After the reaction, stepwise injection extracted a CO_2 fraction using liquid nitrogen and sealed the fraction in a glass vial using liquid nitrogen and a blowtorch. In this way, stepwise injection produced a series of CO_2 fractions constituting a radiocarbon profile.

Graphitization reactors converted the produced CO_2 fractions to graphite using the hydrogen and iron catalyst method (Vogel et al., 1984). A pneumatic press produced AMS cathodes from the graphite powder, and the HVE 1 MV accelerator (Olsen et al., 2017) at Aarhus AMS Centre radiocarbon dated the AMS cathodes. Radiocarbon ages were reported as ^{14}C years BP and fractionation corrected using the d^{13}C calculated from the AMS analysis (Stuiver and Polach, 1977). The online program OxCal 4.4 with the IntCal20 calibration curve was used to calculate calendar dates from radiocarbon ages (Bronk Ramsey, 2009; Reimer et al., 2020).

2.5. Conclusiveness criteria

As explained in materials and methods, stepwise injection produced results in the form of radiocarbon profiles. Conclusiveness criteria then evaluated radiocarbon profiles as conclusive or inconclusive, and only conclusive profiles had a mortar date derived. The conclusiveness criteria are (Daugbjerg et al., 2022; Heinemeier et al., 2010; Lindroos et al., 2018; Ringbom et al., 2014):

CI: The ^{14}C ages of the first two, or more, CO_2 fractions from the same radiocarbon profile agree by a statistical test.

CII: The ^{14}C ages of the first fractions from three, or more, samples from the same building unit agree by a statistical test.
CIII: The ^{14}C ages of the first fractions from two samples from the same building unit agree by a statistical test. (Similar to CII but weaker)
CIV: The ^{14}C age of the first fraction from a sample agrees by a statistical test with another independent date (e.g. wood or charcoal) from the same building unit.

The statistical test used in the criteria was a chi-square test for goodness of fit for the weighted average of the fractions under evaluation (Bennett and Franklin, 1954; Press et al., 1992). When fractions passed a criterion, they had a weighted average with propagated uncertainty and mean with standard deviation calculated. If the propagated uncertainty was greater than the standard deviation, the conclusive age was the weighted average with propagated uncertainty. Else, the conclusive age was the mean with standard deviation.

The conclusiveness criteria exploit that secondary carbonates, binder carbonate and geological carbonates have different reaction rates when dissolving in acid (Daugbjerg et al., 2022; Heinemeier et al., 2010; Lindroos et al., 2007; Lindroos et al., 2018; Ringbom et al., 2014). Here, secondary carbonates react fastest, binder carbonate reacts intermediately and geological carbonates react slowest. The conclusiveness criteria thus attempted to identify the radiocarbon age of the binder in the first fractions of radiocarbon profiles, away from potential contributions from geological carbonates in later fractions. Notice that this attempt may yield an inconclusive result, if geological carbonates and/or secondary carbonates influenced and distorted the first fractions. The conclusiveness criteria are an empirical principle, and Daugbjerg et al. (2022) critically tested them for stepwise injection with 5 mortar samples with known age, and found accurate agreement between conclusive ages and expected ages for 5 out of 5 samples. Heinemeier et al. (2010) critically tested the criteria for sample preparation by sequential dissolution and found accurate agreement between conclusive ages and expected ages for 75 out of 79 samples.

3. Results

Table 1 summarizes results from alkalinity screening, petrography, mortar radiocarbon dating by stepwise injection and conclusiveness criteria.

3.1. Sample characterization

Table 1 shows alkalinity results (ΔpH/m) for mortar samples from the Roman period building with cistern, and the caption of Table 1 states the result for the alkalinity standard (ΔpH/m). In Table 1, the chi-square tests for the alkalinity characterization showed that no samples were significantly different from the standard, i.e. the weighted average of the three stable calcite references. Consequently, there was no suspicion of secondary carbonates from alkalinity.

The carbonaceous character of the binder and a large part of the aggregate, along with the abundant presence of not completely burnt limestone fragments (Fig. 4, Fig. A2B), made these samples difficult in terms of radiocarbon dating. The analyzed samples contained fragments of various carbonate rocks (bioclastic limestone, marly limestone), crushed shells, quartz, chert and many small fragments of ceramics (Fig. 4, Fig. A1, Fig. A2). The proportions of ingredients varied within the samples. The samples: J16-Scd-13-73, J16-Se-43-5, J16-Se-35-5, J16-Sd-13-38 had the highest amounts of carbonate aggregate. The binder of all analyzed samples was carbonate with a slight addition of clay minerals (Fig. A2). The product from calcination of clay may have exhibited pozzolanic activity and may have caused disintegration of the lime grain (Nežerka et al., 2014). The binder was heterogeneous with many fine thermally modified carbonate fragments that were not completely burnt (Fig. 4 E, K) and singular secondary calcite (Fig. 4A).

The map of element distribution (Fig. A2A) shows the composition of the analyzed samples, where Si, Al, Fe, K, Na, Mg and Ti correspond to ceramics fragments, Si to quartz and chert, and Ca correspond to carbonaceous components.

3.2. Radiocarbon dating

Fig. 5 shows examples of radiocarbon profiles from the Roman building in Trench S, and Table 1 lists all radiocarbon profiles. Most radiocarbon profiles had higher ^{14}C ages for later fractions. The characterization results found no alkalinity and geological carbonates for all samples, and petrography found secondary calcite for sample J16-Sa-8-7. These characterization results supported interpreting the radiocarbon profiles, apart from J16-Sa-8-7, as a mixture of binder calcite and slower dissolving geological carbonate. In Table 1, there was one further exception to this situation and that was sample J16-Scd-13-74, which had a decreasing profile. One possible understanding of the radiocarbon profile of J16-Scd-13-74 was a mixture of binder calcite and faster dissolving geological carbonate. The conclusiveness criteria do not apply to such an exception, and the radiocarbon profile of J16-Scd-13-74 was disqualified. The conclusiveness criteria, presented in materials and methods, evaluated the radiocarbon profiles, see Table 1 and Fig. 5. Evaluation of criteria II, III and IV assumed that red painted wall surfaces are from the same building unit, i.e. the wall decoration of the Roman period building. The red painted samples are J16-Sb-23-11, J16-Scd-13-73, J16-Sd-13-38, J16-Sd-22-62 and J16-Se-43-5, displayed in Fig. 3.

4. Discussion

4.1. Characterization

The alkalinity screening found no samples where alkalinity was significantly different from the standard (Table 1). Consequently, alkalinity characterization expected no secondary carbonates from alkalinity for any samples. However, sample J16-Sa-8–7 showed secondary calcite in polarizing light microscopy (Fig. 4A). Furthermore, the radiocarbon profile of sample J16-Sa-8–7 (Table 1), had a first fraction with a ^{14}C age that was significantly younger than any conclusive mortar age in Table 1. Fig. 4A and Table 1 thus support that sample J16-Sa-8–7 had secondary carbonate, while the alkalinity screening failed to detect this. One possible explanation for this failure of detection was that mortar can have secondary carbonate without alkalinity, see Daugbjerg et al., 2021. Another possible explanation was the use of different grain size fractions for alkalinity characterization and preparation for radiocarbon dating, see materials and methods. Considering these results, it was difficult to use alkalinity screening without support from other characterization methods, while petrography seemed more useful at detecting both secondary carbonate and geological carbonate.

Table 1 also summarizes petrography results. All samples had a large amount of carbonaceous aggregate. The presence of incompletely burnt limestone fragments with a thermally changed structure indicated a low temperature or short burning time of the raw material. It could be assumed that it was a soft burning process (Boynton 1980; Yaseen et al., 2013). The exact determination of the provenance of the raw material for the production of mortar and plaster in Jerash was difficult due to the

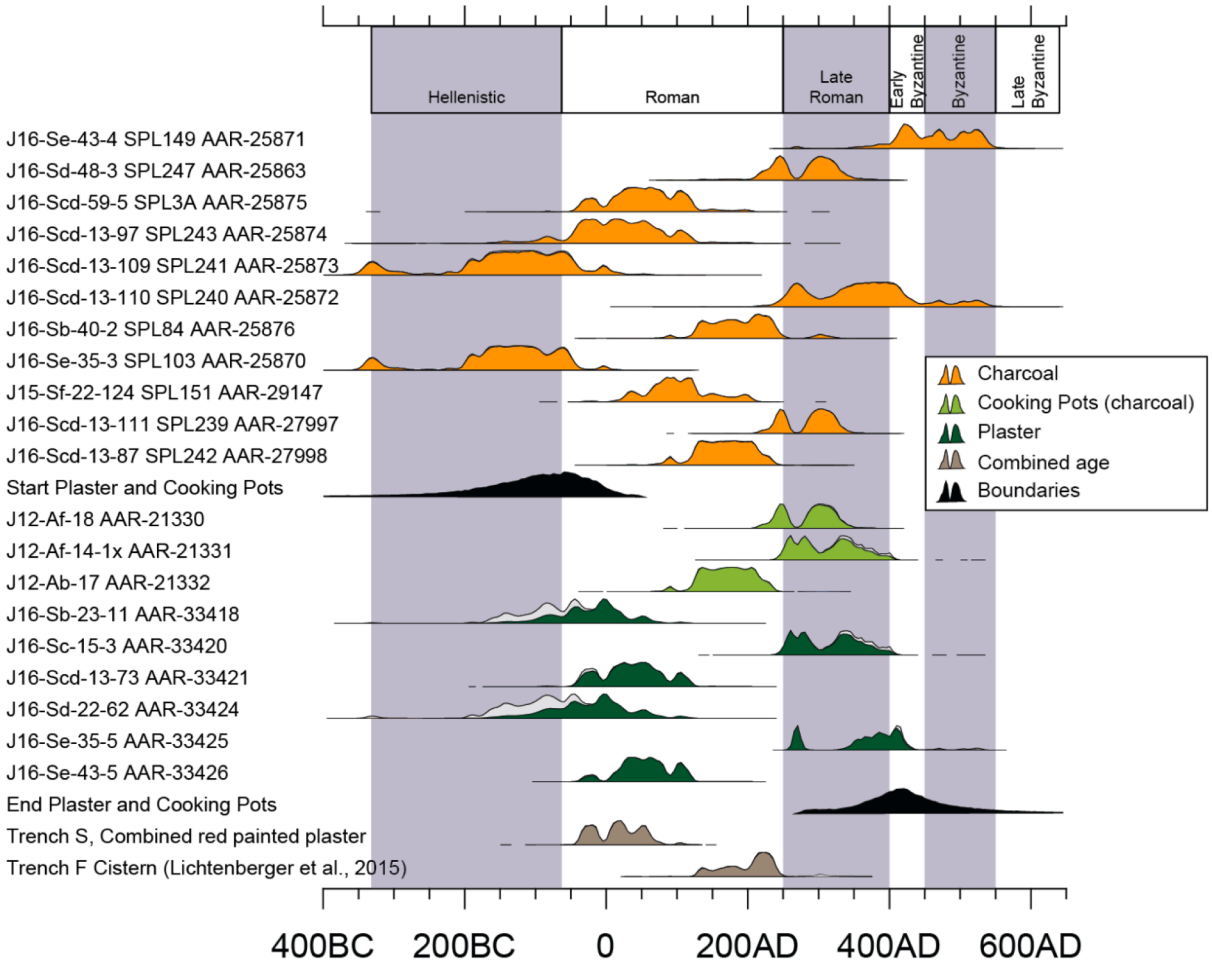

Fig. 6. Calendar dates for conclusive plaster dates. Charcoal dates from Philippsen and Olsen (2020). Phase model with start and end boundaries for plaster and charcoal from cooking pots. Orange is charcoal from Trench S. Light green is cooking pot charcoal from Trench A. Dark green is plaster from Trench S. The red painted plaster dates passed a chi-square test, df = 3 T = 5.9(5% 7.8), and combined to 1995 ± 16 ^{14}C years BP. The mortar date from the cistern in Trench F were taken from Lichtenberger et al. (2015).

abundance of carbonate deposits in the entire region (Abdelhamid, 1995). The sedimentary rock in the vicinity are mainly of Late Cretaceous age (Abed, 1982; Bender, 1974). Based on the characteristics of the mortar and plaster components, the most probable source of material for the production of the analyzed samples seemed to be carbonate formations from the Ajloun Group (Quennell, 1951). The Cenomanian–Turonian Ajloun Group comprises the Naur limestone, Fuheis, Hummar, Wadi Shuayb and Wadi As Sir formations (Masri, 1963). More specifically, referring to petrographic observations and the location of ancient quarries, the raw materials for the production of binders may have come from the Naur limestone crops out at the Al-Shawahed quarry (Abu-Jaber et al., 2009). In order to verify these observations, it would be necessary to collect samples from the surrounding quarries, following the example of the study by Abu-Jaber et al. (2009).

4.2. Conclusiveness criteria

In this study, the conclusiveness criteria derived conclusive binder ages from the radiocarbon profiles in Table 1, and it was interesting to speculate if data modelling or extrapolation also could have done this derivation. Indeed, one could have asked if the conclusive age, calculated as a weighted average or mean, in some situations could have a minor contribution from secondary carbonates or geological carbonates. In such situations, modelling or extrapolation could have been an interesting alternative to the conclusiveness criteria. However, considering the uncertainties of the measured radiocarbon ages, and that fractions passed a statistical test prior to use in calculation of conclusive age, the existence-question of a minor contamination contribution to a conclusive age was not adequately resolved and very difficult to assess. At any rate, this study did not have an appropriate model nor well-restraining data for the reaction rates of a multi carbonate system, and it used the more conservative conclusiveness criteria (Daugbjerg et al., 2022; Heinemeier et al., 2010). For interesting discussions of modelling of radiocarbon profiles from sample preparation by ramped pyroxidation or sequential dissolution see Barrett et al. (2021) or Lindroos et al. (2007), respectively.

4.3. Radiocarbon dating of lime plaster

Fig. 6 shows calibrated dates for the conclusive plaster dates listed in Table 1. The samples J16-Sb-23-11, J16-Scd-13-73, J16-Sd-22-62 and J16-Se-43-5 are red painted wall plaster. Here the plaster dates for J16-

Table 2
Charcoal dates for Trench S, and a phase model for plaster from Trench S and charcoal from Trench A. Charcoal dates from Philippsen and Olsen (2020). Mortar date for Trench F cistern from Lichtenberger et al. (2015).

Lab ID	^{14}C age ^{14}C years BP	Calibrated age 68.2% confidence interval(s)	Calibrated age 95.4% confidence interval(s)	Model agreement	Calibrated age (modelled) 68.2% confidence interval(s)	Calibrated age (modelled) 95.4% confidence interval(s)
J16-Se-43-4 SPL149 AAR-25871	1627 ± 34	410 CE–441 CE [25.4%] 455 CE–479 CE [15.7%] 496 CE–535 CE [27.2%]	377 CE–546 CE [95.4%]	99.3%	411 CE–441 CE [25.9%] 457 CE–479 CE [14.9%] 496 CE–535 CE [27.5%]	377 CE–546 CE [95.4%]
J16-Sd-48-3 SPL247 AAR-25863	1790 ± 31	235 CE–256 CE [23.2%] 286 CE–326 CE [45.1%]	206 CE–363 CE [95.4%]	99.3%	234 CE–256 CE [23.9%] 286 CE–326 CE [44.4%]	206 CE–361 CE [95.4%]
J16-Scd-59-5 SPL3A AAR-25875	1968 ± 35	11 CE–85 CE [54.8%] 96 CE–117 CE [13.5%]	45 BCE–130 CE [94.8%] 146 CE–154 CE [0.6%]	99.6%	11 CE–85 CE [54.8%] 95 CE–117 CE [13.5%]	45 BCE–131 CE [94.8%] 146 CE–154 CE [0.6%]
J16-Scd-13-97 SPL243 AAR-25874	2000 ± 45	43 BCE–70 CE [68.3%]	145 BCE–138 BCE [0.4%] 107 BCE–128 CE [95.0%]	99.8%	43 BCE–70 CE [68.3%]	146 BCE–139 BCE [0.4%] 108 BCE–128 CE [95.0%]
J16-Scd-13-109 SPL241 AAR-25873	2107 ± 50	192 BCE–186 BCE [2.2%] 176 BCE–47 BCE [66.1%]	351 BCE–286 BCE [10.6%] 226 BCE–218 BCE [0.6%] 209 BCE–15 CE [84.2%]	99.9%	191 BCE–187 BCE [1.3%] 176 BCE–47 BCE [67.0%]	351 BCE–286 BCE [10.6%] 225 BCE–217 BCE [0.6%] 209 BCE–16 CE [84.3%]
J16-Scd-13-110 SPL240 AAR-25872	1695 ± 56	256 CE–286 CE [15.1%] 326 CE–420 CE [53.2%]	239 CE–441 CE [86.8%] 452 CE–479 CE [3.3%] 496 CE–535 CE [5.4%]	99.8%	256 CE–286 CE [15.1%] 326 CE–420 CE [53.2%]	239 CE–441 CE [87.1%] 456 CE–480 CE [2.9%] 495 CE–536 CE [5.4%]
J16-Sb-40-2 SPL84 AAR-25876	1850 ± 33	132 CE–142 CE [7.7%] 158 CE–193 CE [26.6%] 200 CE–237 CE [33.9%]	87 CE–94 CE [0.8%] 119 CE–251 CE [92.4%] 296 CE–311 CE [2.2%]	99.8%	132 CE–143 CE [7.8%] 158 CE–193 CE [26.9%] 200 CE–237 CE [33.6%]	89 CE–92 CE [0.4%] 118 CE–251 CE [92.8%] 295 CE–311 CE [2.2%]
J16-Se-35-3 SPL103 AAR-25870	2115 ± 39	174 BCE–87 BCE [53.3%] 79 BCE–52 BCE [15.0%]	348 BCE–308 BCE [8.6%] 205 BCE–38 BCE [85.8%] 10 BCE–3 CE [1.1%]	99.7%	175 BCE–87 BCE [53.4%] 80 BCE–52 BCE [14.9%]	348 BCE–307 BCE [8.6%] 206 BCE–37 BCE [85.8%] 10 BCE–3 CE [1.1%]
J15-Sf-22-124 SPL151 AAR-29147	1930 ± 26	31 CE–41 CE [4.9%] 61 CE–129 CE [63.4%]	25 CE–204 CE [95.4%]	99.7%	31 CE–42 CE [5.1%] 60 CE–130 CE [63.2%]	25 CE–204 CE [95.4%]
J16-Scd-13-111 SPL239 AAR-27997	1784 ± 23	240 CE–255 CE [19.5%] 287 CE–325 CE [48.8%]	221 CE–262 CE [31.5%] 277 CE–339 CE [63.9%]	99.1%	239 CE–255 CE [19.7%] 287 CE–325 CE [48.6%]	221 CE–263 CE [31.7%] 277 CE–340 CE [63.7%]
J16-Scd-13-87 SPL242 AAR-27998	1877 ± 28	130 CE–207 CE [68.3%]	84 CE–97 CE [3.4%] 116 CE–236 CE [92.1%]	99.9%	130 CE–148 CE [16.6%] 153 CE–207 CE [51.6%] 146 BCE–10 BCE [68.3%]	84 CE–97 CE [3.2%] 116 CE–236 CE [92.3%] 280 BCE–27 CE [95.4%]
Start Plaster and Cooking Pots						
J12-Af-18 AAR-21330	1783 ± 25	240 CE–256 CE [19.2%] 286 CE–326 CE [49.1%]	217 CE–264 CE [31.7%] 276 CE–345 CE [63.7%]	99.0%	239 CE–256 CE [20.7%] 286 CE–324 CE [47.5%]	217 CE–264 CE [33.4%] 276 CE–344 CE [62.0%]
J12-Af-14-1x AAR-21331	1739 ± 25	252 CE–293 CE [31.4%] 318 CE–364 CE [36.9%]	247 CE–402 CE [95.4%]	101.1%	251 CE–293 CE [36.7%] 318 CE–358 CE [31.6%]	245 CE–386 CE [95.4%]
J12-Ab-17 AAR-21332	1872 ± 25	130 CE–145 CE [13.9%] 155 CE–211 CE [54.3%]	121 CE–235 CE [95.4%]	99.8%	131 CE–211 CE [68.3%]	119 CE–236 CE [95.4%]
J16-Sb-23-11 AAR-33418	2051 ± 38	102 BCE–14 CE [68.3%]	167 BCE–31 CE [92.4%] 41 CE–61 CE [3.1%]	101.9%	85 BCE–74 BCE [4.8%] 58 BCE–25 CE [63.4%]	141 BCE–134 BCE [0.7%] 123 BCE–73 CE [94.8%]
J16-Sc-15-3 AAR-33420	1735 ± 24	254 CE–289 CE [29.1%] 322 CE–366 CE [37.2%] 372 CE–376 CE [2.0%]	249 CE–298 CE [35.6%] 308 CE–403 CE [59.9%]	101.1%	253 CE–290 CE [34.7%] 322 CE–363 CE [33.6%]	247 CE–392 CE [95.4%]
J16-Scd-13-73 AAR-33421	1983 ± 30	33 BCE–14 BCE [12.4%] 6 CE–75 CE [55.9%]	42 BCE–87 CE [85.2%] 94 CE–119 CE [10.2%]	100.4%	28 BCE–14 BCE [8.4%] 6 CE–77 CE [59.9%]	40 BCE–88 CE [84.7%] 93 CE–119 CE [10.7%]
J16-Sd-22-62 AAR-33424	2058 ± 45	147 BCE–134 BCE [5.2%] 111 BCE–9 CE [63.1%]	193 BCE–185 BCE [0.7%] 177 BCE–66 CE [94.7%]	97.9%	85 BCE–25 CE [68.3%]	146 BCE–78 CE [95.4%]
J16-Se-35-5 AAR-33425	1663 ± 24	366 CE–425 CE [68.3%]	261 CE–279 CE [6.0%] 341 CE–436 CE [85.5%] 466 CE–475 CE [1.2%] 502 CE–508 CE [0.7%] 516 CE–531 CE [2.1%]	81.7%	264 CE–275 CE [14.6%] 365 CE–419 CE [53.7%]	260 CE–280 CE [19.4%] 341 CE–428 CE [76.0%]
J16-Se-43-5 AAR-33426	1967 ± 22	22 CE–81 CE [60.3%] 100 CE–109 CE [8.0%]	31 BCE–14 BCE [5.0%] 7 CE–121 CE [90.4%]	100.5%	22 CE–81 CE [60.3%] 100 CE–110 CE [8.0%] 358 CE–479 CE [68.3%]	30 BCE–15 BCE [3.8%] 6 CE–122 CE [91.7%] 277 CE–586 CE [95.4%]
End Plaster and Cooking Pots						
Trench S, Combined red painted plaster	1995 ± 16	34 BCE–13 BCE [22.9%] 5 CE–29 CE [29.8%] 44 CE–59 CE [15.6%]	42 BCE–73 CE [95.4%]	98.9%	34 BCE–13 BCE [22.1%] 5 CE–30 CE [29.6%] 43 CE–60 CE [16.6%]	41 BCE–71 CE [95.4%]
Trench F Cistern (Lichtenberger et al., 2015)	1841 ± 23	167 CE–188 CE [14.9%] 202 CE–241 CE [53.4%]	127 CE–246 CE [95.4%]	99.3%	165 CE–188 CE [15.7%] 202 CE–241 CE [52.6%]	127 CE–246 CE [95.4%]

Sb-23-11 and J16-Sd-22-62 spanned from the middle of the 2nd century BCE to the early 1st century CE. Plaster dates for J16-Scd-13-73 and J16-Se-43-5 spanned from the late 1st century BCE to the early 2nd century CE. The samples J16-Sc-15-3 and J16-Se-35-5 had later calibrated dates, with probability distributions in the Late Roman era (250–400 CE) and the Early Byzantine era (400–450 CE).

The results of the plaster dates showed two clear phases – one, which must correspond with the construction of the complex, and firmly dated to between the 1st century BCE and the 1st century CE. A weighted average combined the plaster dates from the red wall surfacing with chi-square df = 3 T = 5.9(5% 7.8) and value 1995 ± 16 ^{14}C years BP, which calibrated to 42 BCE – 73 CE (95.4 %) (see Fig. 6 and Table 2), which we state for the construction date of the cistern. The other phase of plaster samples dated to the 3rd–5th centuries CE and indicated that the complex was closed off then or later, since the dates relate to elements, which had been part of the building complex and was filled into the cistern in the backfill process. Usually cisterns had to be renovated and re-plastered over time, and the second phase starting in the 3rd century CE probably relates to this last phase of reparation.

Lichtenberger and Raja (2015) discuss the filling of the cistern, as excavated in Trench A. The fill features homogenous layers of earth, larger stones or smaller stones, which supports a rapid filling event. Furthermore, the filling contained an intentional deposition of cooking pots filled with ash, glass sherds, ceramic sherds and animal bones. Lichtenberger and Raja (2015) discuss several possible explanations, for example magical practices or a termination ritual also attested in other places in the region in the 2nd–4th centuries CE. Overall, the ritual and homogenous fill layers suggest a single, rapid, intentional filling event, most likely coinciding with the destruction of the building.

Philippsen and Olsen (2020) present charcoal radiocarbon dates from Trench S and Trench A. They also discuss re-deposition and old wood effect for charcoal and formulate models that allow some correction for charcoal samples with an inherent age. They present charcoal dates from the content of the deposited cooking pots in Trench A, and a model that dates the deposition of cooking pots to 220–421 CE (95.4 %). Philippsen and Olsen (2020) also present a model for charcoal dates in Trench S associated with the cistern fill. This model shows that activity at the cistern may start as far back as the 2nd century BCE, and it stops in the 3rd century CE or later.

Fig. 6 and Table 2 show radiocarbon dates from charcoal and plaster in Trench S and Trench A. The span of the plaster dates was similar to the span of the charcoal dates in Trench A and Trench S presented by Philippsen and Olsen (2020). Emphasizing the context of the mortar samples in the homogenous fill of the cistern, one could argue that the entire fill, including associated charcoal samples, is younger than the mortar dates. This could support the charcoal re-deposition and rapid fill discussed by Philippsen and Olsen (2020) and Lichtenberger and Raja (2015).

The radiocarbon dates from plaster and the cooking pots are less vulnerable to re-deposition and bioturbation than the charcoal dates from Trench S. Therefore OxCal made a simple phase model for dates from plaster and cooking pots to assess the start and end of activity at the cistern complex (Bronk Ramsey, 2009). This model found activity starting in 280 BCE–27 CE (95.4 %), and ending at 277–586 CE (95.4 %), see Fig. 6 and Table 2 for further details. Overall, these start and end dates agreed with the results from Lichtenberger and Raja (2015) and Philippsen and Olsen (2020), albeit here the start and end intervals were somewhat narrower implying greater certainty. We therefore state that the cistern fill event took place sometime after 277 CE, i.e. late 3rd century CE.

Lichtenberger et al. (2015) present mortar dating from another cistern on the south slope of the Northwest Quarter, see Trench F in Fig. 1. There mortar from the initial phase of the cistern in Trench F dates to 1841 ± 23 ^{14}C years BP, which calibrates to 127–246 CE (95.4 %) (see Fig. 6 and Table 2). Afterwards, the cistern in Trench F was in use, with multiple phases, until the 6th–7th century CE (Lichtenberger et al., 2015). In Trench S, the combined age of red painted plaster samples inferred the date of construction of the cistern (see Fig. 6 and Table 2). The radiocarbon ages of the two cisterns failed a chi-square test for goodness of fit with df = 1 T = 30 (5% 3.8), and thus the cistern in Trench S was significantly older than the cistern in Trench F. From the construction of the cistern in Trench F (127–246 CE (95.4 %)) to the filling of the Trench S cistern (277–586 CE (95.4 %)), the two cisterns coexisted. Given the calendar date distributions, the period of coexistence ranged from several decades to several centuries (see Fig. 6 and Table 2). Perhaps, they simultaneously supplied water to different parts of ancient Gerasa at different elevations (see the elevation contours in Fig. 1).

5. Conclusion

It was challenging to radiocarbon date mortar and plaster from ancient Gerasa, especially because the aggregate contained grains from the local limestone geology, which contaminated the mortar dating effort with geological carbonate (Lichtenberger et al., 2015). Daugbjerg et al. (2022) present methodology with stepwise injection, which improves Jerash mortar dating compared to sequential dissolution in Lichtenberger et al. (2015). This methodological improvement also benefitted this study, which presented 6 conclusive radiocarbon profiles out of 10 radiocarbon profiles.

The presented mortar dating results divided into two categories. First, red painted wall plaster samples that dated from the middle of the 2nd century BCE to the 1st century CE. The ages of these samples had significant agreement, and their combined age indicated a construction event somewhere from the last half of the 1st century BCE to the middle of the 1st century CE. The second category were samples of unpainted plaster, and they indicated a later construction or renovation event in the 3rd–5th century CE. They constrained the date of filling and closure of the cistern to sometime after the late 3rd century CE.

The date of closure of the cistern that was based on plaster and cooking pots, 277–586 CE (95.5 %), largely agreed with the chronologies based on charcoal by Philippsen and Olsen (2020). Compared to charcoal dating, plaster dating improved knowledge of the absolute date for construction of the cistern in Trench S and provided a more restricted interval, 42 BCE–73 CE (95.4 %).

CRediT authorship contribution statement

Thomas Schrøder Daugbjerg: Conceptualization, Methodology, Investigation, Formal analysis, Writing – original draft, Writing – review & editing, Visualization. **Achim Lichtenberger:** Conceptualization, Resources, Project administration, Funding acquisition, Writing – review & editing. **Alf Lindroos:** Conceptualization, Resources, Writing – review & editing. **Danuta Michalska:** Conceptualization, Resources, Investigation, Formal analysis, Writing – review & editing. **Rubina Raja:** Conceptualization, Supervision, Resources, Writing – review & editing, Project administration, Funding acquisition. **Jesper Olsen:** Conceptualization, Supervision, Writing – review & editing, Project administration.

Acknowledgements

The work of the Danish-German Jerash Northwest Quarter Project was supported by the Carlsberg Foundation, the Danish National Research Foundation under the grant DNRF119 – Centre of Excellence for Urban Network Evolutions (UrbNet), Deutsche Forschungsgemeinschaft, Deutscher Palästina-Verein, the EliteForsk initiative of the Danish Ministry of Higher Education and Science and H. P. Hjerl Hansens Mindefondet for Dansk Palæstinaforskning.

Appendix

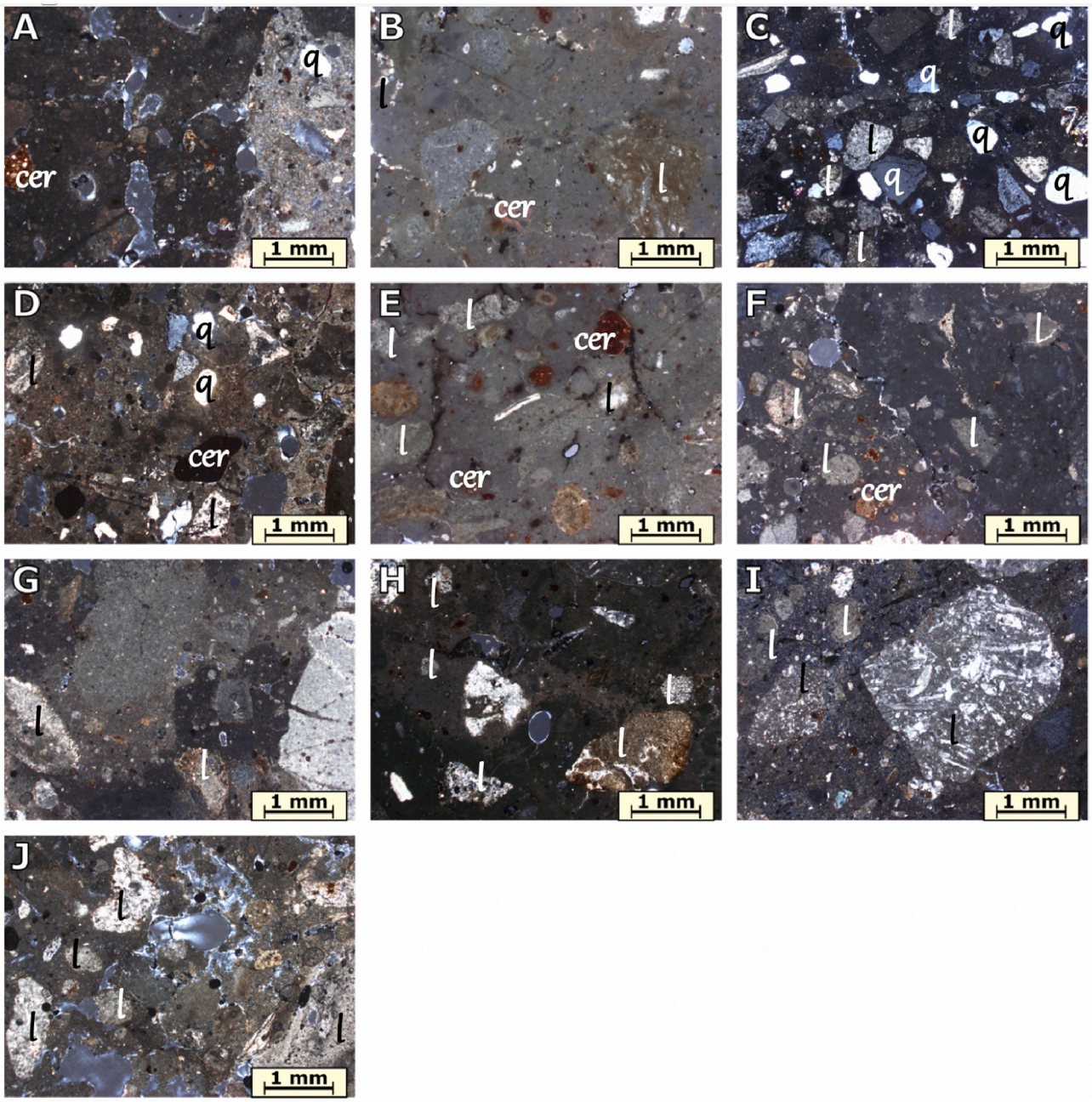

Fig. A1. Microphotographs of analyzed samples in the same magnification. Petrographic identifications: l – carbonaceous components; cer – ceramic fragments; q – quartz. **A** Sample J16-Sa-8-7, two layers of plaster. The first layer is brownish and rich in small fragments of ceramics. The binder is also rich in clay minerals or ceramic dust. The second layer has less clay admixtures and fragments of ceramics. **B** Sample J16-Sb-23-11, large pieces of carbonaceous aggregate and fine fragments in the binder. There are also small pieces of ceramics throughout the sample. **C** Sample J16-Sbc-48-6, numerous aggregates, quartz, single pieces of chert, shell fragments, and limestone. **D** Sample J16-Sc-15-3, quartz, ceramics and carbonaceous fragments of aggregate. **E** Sample J16-Scd-13-73, many fragments of incompletely burnt limestone, small fragments of ceramics, shells. **F** Sample J16-Scd-13-74, a large amount of carbonate aggregate of different size and small pieces of ceramics. **G** Sample J16-Sd-13-38, carbonaceous aggregate, including numerous not entirely burnt fragments, single small fragments of ceramics and grains of chert. **H** Sample J16-Sd-22-62, carbonate binder with clay minerals and small ceramic fragments within the sample. **I** Sample J16-Se-35-5, sample almost completely carbonaceous, a lot of unburned fragments and small pieces of crushed ceramics. **J** Sample J16-Se-43-5, both binder and aggregate have a carbonaceous character.

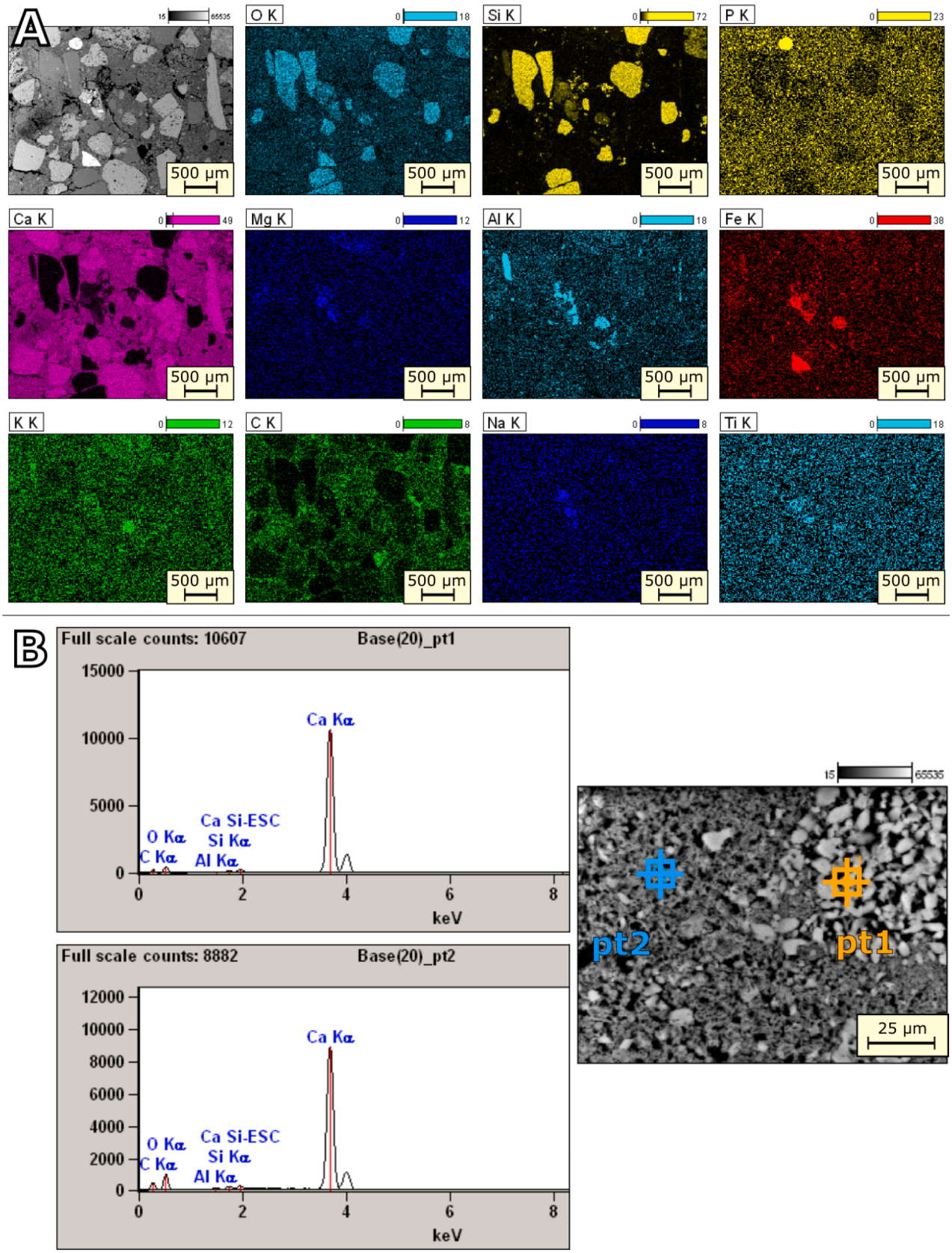

Fig. A2. SEM-EDS analyses of selected samples. **A** Spectral imaging of sample J16-Sbc-48-6. **B** EDS spectra of carbonaceous aggregate (pt1) and lime binder (pt2) together with SEM image of the sample J16-Sd-22-62.

References

Abdelhamid, G., 1995, The Geology of Jarash Area, Map Sheet No. 3154-I, Bulletin 30: Natural Resources Authority, Amman: Jordan.

Abed, A.M., 1982. Microfacies and paleoenvironment of the Wadi Sir Formation (Upper Cretaceous), North Jordan. *Facies* 7 (1), 229–235.

Abu-Jaber, N., al Saad, Z., Smadi, N., 2009. The quarryscapes of Gerasa (Jarash), Jordan., *Geological Survey of Norway, Special Publication 12*, 67-77.

Al-Bashaireh, K., 2013. Plaster and mortar radiocarbon dating of Nabatean and Islamic structures, South Jordan. Archaeometry 55 (2), 329–354.

Al-Bashaireh, K., 2015. Radiocarbon age determinations of mosaic mortar layers Of Churches from North Jordan. Radiocarbon 57 (5), 851–863.

al-Nahar, M., 2010, Tell Abu Suwwan, A neolithic site in jordan: preliminary report on the 2005 and 2006 Field Seasons, *Bull. Am. Schools Orient. Res.*, **357**, 1-18.

al-Nahar, M., 2018, The Neolithic Site of Tell Abu Suwwan in Jerash, Jordan, in *The Archaeology and History of Jerash, 110 Years of Excavations*, A. Lichtenberger, and R. Raja, eds., Jerash Papers (JP 1), Brepols Publishers, Turnhout.

Barrett, G.T., Keaveney, E., Lindroos, A., Donnelly, C., Daugbjerg, T.S., Ringbom, Å., Olsen, J., Reimer, P.J., 2021. Ramped pyroxidation: A new approach for radiocarbon dating of lime mortars. J. Archaeol. Sci. 129, 105366.

Baxter, M.S., Walton, A., 1970. Radiocarbon dating of mortars. Nature 225 (5236), 937–938.

Bender, F., 1974, Geology of Jordan: Berlin, Borntraeger.

Bennett, C.A., Franklin, N.L., 1954. Statistical Analysis in Chemistry and the Chemical Industry. Wiley, New York.

Boaretto, E., 2009. Dating materials in good archaeological contexts: the next challenge for radiocarbon analysis. Radiocarbon 51 (1), 275–281.

Boyer, D.D., 2019, An Analysis of the Historical Water Management System to Gerasa in the period 100 BC to AD 700.

Boynton, R.S., 1980. Chemistry and Technology of Lime and Limestone. Wiley & Sons, New York.

Bronk Ramsey, C., 2009. Bayesian analysis of radiocarbon dates. Radiocarbon 51 (1), 337–360.

Daugbjerg, T.S., Lindroos, A., Heinemeier, J., Ringbom, Å., Barrett, G., Michalska, D., Hajdas, I., Raja, R., Olsen, J., 2021. A field guide to mortar sampling for radiocarbon dating*. Archaeometry 63 (5), 1121–1140.

Daugbjerg, T.S., Lindroos, A., Lichtenberger, A., Raja, R., Lichtenberger, A., 2022. Revisiting radiocarbon dating of lime mortar and lime plaster from Jerash in Jordan: Sample preparation by stepwise injection of diluted phosphoric acid. Journal of Archaeological Science: Reports 41, 103244.

Folk, R.L., Valastro, S., 1976. Successful Technique for Dating of Lime Mortar by Carbon-14. Journal of Field Archaeology 3 (2), 195–201.

Goslar, T., Nawrocka, D., Czernik, J., 2009. Foraminiferous limestone in 14C dating of mortar. Radiocarbon 51 (3), 987–993.

Heinemeier, J., Jungner, H., Lindroos, A., Ringbom, Å., von Konow, T., Rud, N., 1997. AMS C-14 dating of lime mortar. Nucl. Instrum. Methods Phys. Res. Sect. B-Beam Interact. Mater. Atoms 123 (1–4), 487–495.

Heinemeier, J., Ringbom, Å., Lindroos, A., Sveinbjornsdottir, A.E., 2010. Successful AMS C-14 dating of non-hydraulic lime mortars from the medieval churches of the Aland Islands Finland. Radiocarbon 52 (1), 171–204.

Kehrberg, I., 2001. A critical look at typologies of ceramics produced in the Late Roman Period at Jarash. In: Studies in the History and Archaeology of Jordan. Department of Antiquities of Jordan, Amman, pp. 601–605.

Kennedy, D., 2007, Gerasa and the Decapolis. A 'Virtual Island' in Northwest Jordan.: London, Duckworth.

Kraeling, C.H., 1938. Gerasa, City of the Decapolis: New Haven. American Schools of Oriental Research, Connecticut.

Labeyrie, J., Delibrias, G., 1964. Dating of old mortars by carbon-14 method. Nature 201 (492), 742.

Lichtenberger, A., 2003. Kulte und Kultur der Dekapolis. Untersuchungen zu numismatischen, archäologischen und epigraphischen Zeugnissen. Harrassowitz Verlag, Wiesbaden.

Lichtenberger, A., Raja, R., 2015. Intentional cooking pot deposits in Late Roman Jerash (Northwest Quarter). Syria (92), 309–328.

Lichtenberger, A., Raja, R., 2016a. Geras in the Middle Islamic period connecting texts and archaeology through new evidence from the Northwest Quarter. Zeitschrift Des Deutschen Palastina-Vereins 132 (1), 63–81.

Lichtenberger, A., Raja, R., 2016b. Living with and on the river-side. The example of Roman Antioch-on-the-Chrysorrhoas-formerly-called-Gerasa, in *Water of Life: Essays from a symposium held on the occasion of Peder Mortensen's 80th birthday*, 98-115, J. K. Madsen, N. O. Andersen, and I. Thuesen, eds., Forlaget Orbis, Copenhagen.

Lichtenberger, A., Raja, R., 2018. Middle Islamic Jerash through the lens of the Longue Dureé, in *Middle Islamic Jerash (9th century - 15th century) Archaeology and History of an Ayyubid-Mamluk settlement*, 5-36, A. Lichtenberger, and R. Raja, eds., Jerash Papers (JP 3), Brepols Publishers, Turnhout.

Lichtenberger, A., Raja, R. (Eds.), 2020a. Hellenistic and Roman Gerasa: the archaeology and history of a Decapolis city: Jerash Papers (JP 5). Brepols Publishers, Turnhout.

Lichtenberger, A., Raja, R., 2020b. Management of water resources over time in semiarid regions: The case of Gerasa/Jerash in Jordan. WIREs Water 7 (1), e1403.

Lichtenberger, A., Lindroos, A., Raja, R., Heinemeier, J., 2015. Radiocarbon analysis of mortar from Roman and Byzantine water management installations in the Northwest Quarter of Jerash, Jordan. *J. Archaeol. Sci.-Rep.* 2, 114–127.

Lichtenberger, A., Raja, R., Stott, D., 2019. Mapping Gerasa: a new and open data map of the site. Antiquity 93 (367), e7.

Lindroos, A., Heinemeier, J., Ringbom, Å., Brasken, M., Sveinbjornsdottir, A., 2007. Mortar dating using AMS C-14 and sequential dissolution: Examples from medieval, non-hydraulic lime mortars from the Åland Islands, SW Finland. Radiocarbon 49 (1), 47–67.

Lindroos, A., Heinemeier, J., Ringbom, Å., Brock, F., Sonck-Koota, P., Pehkonen, P., Suksi, J., 2011. Problems in radiocarbon dating of Roman pozzolana mortars. Commentationes Humanarum Litterarum 214–230.

Lindroos, A., Ringbom, Å., Heinemeier, J., Hodgins, G., Sonck-Koota, P., Sjöberg, P., Lancaster, L., Kaisti, R., Brock, F., Ranta, H., Caroselli, M., Lugli, S., 2018. Radiocarbon dating historical mortars: lime lumps and/or binder carbonate? Radiocarbon 60 (3), 875–899.

Lindroos, A., Ringbom, Å., Heinemeier, J., Hajdas, I., Olsen, J. 2020. Delayed hardening and reactivation of binder calcite, common problems in radiocarbon dating of lime mortars, *Radiocarbon*, 1-13.

MacLeod, G., Hall, A.J., Fallick, A.E., 1991. Mechanism of carbonate mineral growth on concrete structures as elucidated by carbon and oxygen isotope analyses. Chem. Geol. 86, 335–343.

Marzaioli, F., Nonni, S., Passariello, I., Capano, M., Ricci, P., Lubritto, C., De Cesare, N., Eramo, G., Castillo, J.A.Q., Terrasi, F., 2013. Accelerator mass spectrometry C-14 dating of lime mortars: Methodological aspects and field study applications at CIRCE (Italy). Nucl. Instrum. Methods Phys. Res. Sect. B-Beam Interact. Mater. Atoms 294, 246–251.

Masri, M.R., 1963. The Geology of the Amman-Zarqa Area. Central Water Authority, Ministry of Water and Irrigation, Amman.

Michalska, D., 2019. Influence of different pretreatments on mortar dating results. Nucl. Instrum. Methods Phys. Res. Sect. B-Beam Interact. Mater. Atoms 456, 236–246.

Millipore E.M.D., 2013. Milli-Q® Integral Water Purification Systems: Darmstadt. Merck KGaA, Germany.

Nawrocka, D., Czernik, J., Goslar, T., 2009. C-14 Dating of carbonate mortars from Polish and Israeli sites. Radiocarbon 51 (2), 857–866.

Nawrocka, D., Michniewicz, J., Pawlyta, J., Pazdur, A., 2005. Application of radiocarbon method for dating of lime mortars. Geochronometria 24, 109–115.

Nežerka, V., Slížková, Z., Tesárek, P., Plachý, T., Frankeová, D., Petráňová, V., 2014. Comprehensive study on mechanical properties of lime-based pastes with additions of metakaolin and brick dust. Cem. Concr. Res. 64, 17–29.

Olsen, J., Tikhomirov, D., Grosen, C., Heinemeier, J., Klein, M., 2017. Radiocarbon analysis on the new AARAMS 1MV Tandetron. Radiocarbon 59 (3), 905–913.

Philippsen, B., Olsen, J., 2020. Radiocarbon dating and Bayesian modelling. In: Lichtenberger, A., Raja, R. (Eds.), Environmental Studies, Remote Sensing, and Modelling: Final Publications from the Danish-German Jerash Northwest Quarter Project. Brepols Publishers.

Press, W.H., Teukolsky, S.A., Vetterling, W.T., Flannery, B.P., 1992. Numerical Recipes in C The Art of Scientific Computing. Cambridge University Press, Cambridge.

Quennell, A.M., 1951. The geology and mineral resources of (former)Trans-Jordan. Col. Geol. Miner. Resour. 2, 85–115.

Raja, R., 2012. Urban Development and Regional Identity in the Eastern Roman Provinces, 50 BC–AD 250: Aphrodisias, Ephesos, Athens. MuseumTusculanum Press, Copenhagen, Gerasa.

Reimer, P.J., Austin, W.E.N., Bard, E., Bayliss, A., Blackwell, P.G., Bronk Ramsey, C., Butzin, M., Cheng, H., Edwards, R.L., Friedrich, M., Grootes, P.M., Guilderson, T.P., Hajdas, I., Heaton, T.J., Hogg, A.G., Hughen, K.A., Kromer, B., Manning, S.W., Muscheler, R., Palmer, J.G., Pearson, C., van der Plicht, J., Reimer, R.W., Richards, D.A., Scott, E.M., Southon, J.R., Turney, C.S.M., Wacker, L., Adolphi, F., Büntgen, U., Capano, M., Fahrni, S.M., Fogtmann-Schulz, A., Friedrich, R., Köhler, P., Kudsk, S., Miyake, F., Olsen, J., Reinig, F., Sakamoto, M., Sookdeo, A., Talamo, S., 2020. The IntCal20 Northern Hemisphere radiocarbon age calibration curve (0–55 cal kBP). Radiocarbon 62 (4), 725–757.

Ringbom, Å., Lindroos, A., Heinemeier, J., Sonck-Koota, P., 2014. 19 Years of mortar dating: learning from experience. Radiocarbon 56 (2), 619–635.

Seigne, J., 1992. Jérash romaine et byzantine: Développement urbain d'une ville provinciale orientale. Stud. Hist. Archaeol. Jordan 331–341.

Seigne, J., 2004, Remarques préliminaires à une étude sur l'eau dans la Gerasa antique, in *Men of Dikes and Canals: The Archaeology of Water in the Middle East. International symposium held at Petra, Wadi Musa (H.K. of Jordan) 15–20 June, 1999*, 173-85, H.-D. Bienert, and J. Häser, eds., Marie Leidorf, Rahden.

Stott, D., Kristiansen, S.M., Lichtenberger, A., Raja, R., 2018. Mapping an ancient city with a century of remotely sensed data. Proc. Natl. Acad. Sci. 115 (24), E5450–E5458.

Stuiver, M., Polach, H.A., 1977. Reporting OF C-14 Data - Discussion. Radiocarbon 19 (3), 355–363.

Stuiver M., Smith C.S., 1965. Radiocarbon dating of ancient mortar and plaster. Proceedings of the 6th international conference on radiocarbon and tritium dating, Chatters, R.M., Olson E.A., eds. Washington D.C., Clearinghouse for Fed. Sci. & Tech. Inf., Natural Bur. Standards, U.S. Dept. Commerce, pp. 338–343.

Thomsen, K.D., 2019. Urban Life in Jerash, Jordan: The technological and Stylistic Development of Mortar, Plaster and Wall Paintings from Roman Times to the Middle Islamic Period from an Archaeological and Geoarchaeological Perspective (PhD dissertation). Aarhus University, Aarhus.

Tirelli, G., Lugli, S., Galli, A., Hajdas, I., Lindroos, A., Martini, M., Maspero, F., Olsen, J., Ringbom, Å., Sibilia, E., Caroselli, M., Silvestri, E., Panzeri, L., 2020. Integrated dating of the construction and restoration of the Modena Cathedral Vaults (Northern Italy): preliminary results. Radiocarbon 62 (3), 667–677.

Toffolo, M.B., Regev, L., Mintz, E., Kaplan-Ashiri, I., Berna, F., Dubernet, S., Yan, X., Regev, J., Boaretto, E., 2020. Structural characterization and thermal decomposition of lime binders allow accurate radiocarbon age determinations of aerial lime plaster. Radiocarbon 62 (3), 633–655.

Uscatescu, A., 1996. La cerámica del Macellum de Gerasa (Ŷaraš, Jordania). Ministerio de Educación, Cultura y Deporte, Madrid.

Van Strydonck, M., Dupas, M., Dauchotdehon, M., Pachiaudi, C., Marechal, J., 1986. The Influence of contaminating (fossil) carbonate and the variations of delta-C-13 in mortar dating. Radiocarbon 28 (2A), 702–710.

Van Strydonck, M., Vanderborg, K., Dejong, A.F.M., Keppens, E. 1992. Radiocarbon dating of lime fractions and organic material from buildings, *Radiocarbon*, **34(3)**, 873-879.

Vogel, J.S., Southon, J.R., Nelson, D.E., Brown, T.A., 1984. Performance of catalytically condensed carbon for use in accelerator mass-spectrometry. Nucl. Instrum. Methods Phys. Res. Sect. B-Beam Interact. Mater. Atoms 5 (2), 289–293.

WTW, 2017. SenTix® 950/980/Micro 900(-P). Xylem Analytics Germany, Weilheim, Germany.

Yaseen, I.A.B., Al-Amoush, H., Al-Farajat, M., Mayyas, A., 2013. Petrography and mineralogy of Roman mortars from buildings of the ancient city of Jerash, Jordan. Constr. Build. Mater. 38, 465–471.

Zayadine, F., 1986, Jerash Archaeological Project 1981–1983, v. I: Amman, Department of Antiquities of Jordan.